Substrate Mediated Short- and Long-Range Adsorption Patterns of CO on Ag(110)

Wai-Leung Yim[1,*] and Thorsten Klüner[2]

[1]*Institute of High Performance Computing, Agency for Science, Technology, and Research, 1 Fusionopolis Way, No. 16-16 Connexis, Singapore 138632*

[2]*Institut für Reine und Angewandte Chemie, Theoretische Chemie, Carl von Ossietzky Universität Oldenburg, 26129 Oldenburg, Germany*

(Received 16 October 2012; revised manuscript received 14 March 2013; published 7 May 2013)

The adsorption of CO on Ag(110) was recently explained using substrate mediated intermolecular interactions, but the underlying mechanism remains unclear. This study investigates both short- and long-range relaxation patterns for CO adsorption on Ag(110) surfaces and suggests that the relaxation mode can be explained by the interaction of heavy electrons on metal substrates in electron momentum space. The long-range relaxation mode for CO on Ag(110) involved a (6×6) commensurate phase, whereas the short-range relaxation involved an alleviation of Fermi surface nesting along the $\langle 1\bar{1}0 \rangle$ direction of the Ag(110) substrate. The symmetry broken ground state structure at high CO coverage from this work is consistent with the interpretation of available experimental data at low temperature.

DOI: 10.1103/PhysRevLett.110.196101 PACS numbers: 68.35.Ja, 71.18.+y, 73.20.−r

The coverage dependence of self-assembled monolayer structure and its surface chemical reactivity has been studied extensively because of its usefulness in, e.g., catalysis, electrochemistry, and bioelectronics [1–3]. It has been established that the adsorbate coverage affects both the surface chemical composition and the molecular orientation of adsorbates. This might influence precursor-mediated reaction processes [2,4]; e.g., the effect of CO coverage on the adsorption geometry has been reported for Mo, Ni, Cu, Pd, Ag, and Pt substrates [4–9]. Hofmann *et al.* and Bare *et al.* found that in the Pt(110)/CO(2×1) structure the CO molecular axis direction was tilted 26° away from the surface normal between [211] and [433] [5]. Wesner *et al.* observed that CO adsorbates at high coverage were tilted by 21° and 32° on clean and K-covered Ni(110) surfaces, respectively [7]. Electron stimulated desorption ion angular distribution (ESDIAD) experiments by Lee *et al.* showed that at CO coverage of 0.5 ML the CO molecules were tilted by 26° on Ag(110) surfaces [9]. A short-range repulsion model between nearest neighbor CO molecules is accepted as the cause to explain the CO orientation observed experimentally [6,8,9].

While the theory of self-assembled monolayers on metal surfaces has been established based on classical chemical bonding and nonbonding concepts, the physical interpretation of substrate-adsorbate interactions lacks a coherent interpretation [10]. Theoretical investigations of the electron-electron interactions in electron momentum space can bridge the understanding between short-range versus long-range patterns for simple molecules on metal surfaces, which otherwise cannot be explained experimentally [9,11]. We report the findings of an investigation of CO adsorption on Ag(110) by Fermi surface and phonon calculations. The results suggested that (i) invoking CO-CO repulsion can only *partially* explain the tilted orientation of CO on Ag(110), and (ii) accounting for the repulsion between heavy electrons by Fermi surface nesting in $\mathbf{k}$ space, or alleviation of the Fermi surface nesting beyond the conventional chemical bonding concepts, explains more satisfactorily the observed data of a tilted CO orientation at high coverage on Ag(110). Moreover, a long-range commensurate phase induced by the adsorbed CO molecules is predicted for this system for the first time. The long-range phase is favored by reducing metal-$d \rightarrow$ CO-$2\pi^*$ donation.

Direct ESDIAD data comparison was carried out by performing *ab initio* molecular dynamics (AIMD) simulations for CO adsorbing on both sides of slabs of five layer thickness [9,12] (see the Supplemental Material [13]), with the CO-axis orientation projected onto a hemisphere. Several slabs of different coverage and adsorption patterns were selected [Figs. 1(a)–1(c)]. For (2×1) 0.5 ML CO/Ag(110), the CO axis exhibits a two-lobe feature of the probability density [Fig. 1(d)] which suggests CO-CO interactions along the $\langle 001 \rangle$ direction. To yield a reduced intermolecular CO interaction along the $\langle 001 \rangle$ direction, the (2×2) adsorption pattern was considered in which the adjacent rows along the $\langle 1\bar{1}0 \rangle$ direction were shifted by half of the unit cell [Fig. 1(b)]. A pronounced preference of tilted CO species is still maintained [Fig. 1(e)]. The CO axis is also bent by considering the (2×2) adsorption pattern at $\Theta = 0.25$ ML [Figs. 1(c) and 1(f)]. The CO axis bending along the $\langle 001 \rangle$ direction is governed by the CO line density along the $\langle 1\bar{1}0 \rangle$ direction, and the computed CO orientation is consistent with the previous ESDIAD data [9]. Smaller CO coverages with smaller CO line densities at $\Theta = 0.25$ ML were also considered, where the CO axis preferred the perpendicular orientation.

To understand CO tilting preference, the two-dimensional Fermi surface topology must be considered because computation has shown that the allowed relaxation

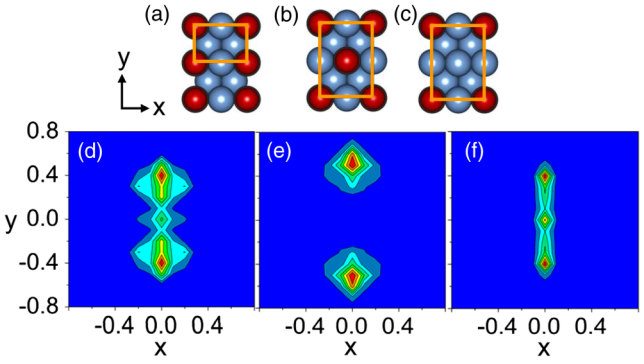

FIG. 1 (color online). Selected adsorption patterns: (a), (b) (2×1) and (2×2), coverage of $\Theta = 0.5$ ML, and (c) (2×2), $\Theta = 0.25$ ML. Projection of CO bond axis orientation: (d), (e) (2×1) and (2×2), $\Theta = 0.5$ ML, and (f) (2×2), $\Theta = 0.25$ ML. x and y directions are along $\langle 1\bar{1}0 \rangle$ and $\langle 001 \rangle$, respectively.

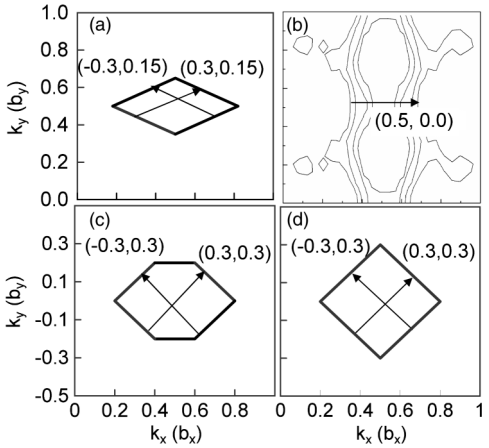

FIG. 2. Fermi surface nesting. (a), (b) (2×1) and commensurate (4×1), both at $\Theta = 0.5$ ML, (c) (2×2), $\Theta = 0.5$ ML, and (d) (2×2), $\Theta = 0.25$ ML. See remarks in Fig. 1.

modes involving phonons were implicated in the two-dimensional Fermi surfaces [14]. Note that Fermi surface nesting can be referenced to the electron-scattering surface state perturbation mechanism [15–18] and is a special case where the Fermi surface shows two highly parallel electronic flatbands denoted by $\mathbf{k}$ and $\mathbf{k}'$ in the Brillouin zone. When the phonon nesting vector is absorbed (or emitted) under the condition $\mathbf{k}\text{-}\mathbf{k}' = \mathbf{q}$, the two flatbands would be brought together leading to a strong Coulombic repulsion of the localized heavy electron [effective mass $m^* = \hbar^2[d^2\epsilon(k)/dk^2]^{-1}$]. As a result, lattice distortion or orbital rehybridization may happen with energy lowering to avoid the Coulombic repulsion. Lau and Kohn predicted that the interaction energy between two adsorbates is linearly proportional to the effective mass of the electron based on second-order perturbation theory [18]. Structural distortion occurs when the amount of energy lowering by electronic energy [$\sum \epsilon(k)$] is larger than the rise of the lattice energy. CO coverage is another factor of distortion because it governs the degree of electron transfer between adsorbates and substrate, the orbital hybridization at CO/Ag(110) interface and the Fermi surface nesting.

Thus, four representative structures were selected to explore the CO line density effect on the two-dimensional Fermi surface [19]. As shown in Fig. 2, the nesting $\mathbf{q}$ vectors [20] were identified. Similar to the AIMD results, Fermi surface nesting happened when the CO-line density along the $\langle 1\bar{1}0 \rangle$ direction reached 0.5 [Figs. 2(a), 2(c), and 2(d)]. The driving force of structure distortion originates from the alleviation of the Fermi surface nesting which results in formation of commensurate structure. Two adsorption patterns have been identified. The long-range pattern (6×6) is newly discovered in this work while the short-range pattern (4×1) has been observed experimentally [9]. The explanation of these patterns is presented below.

In principle, the Fermi surface nesting vector indicates the necessary periodicity of the newly formed commensurate structure. Even though the Fermi surface nesting was considered in the Brillouin zone, the information obtained by the nesting $\mathbf{q}$ vector can be projected to the real space by coordinate transformation. The nesting vector is related to the new periodicity as $N_{\text{cell}} = 1/\|\mathbf{q}\|$. For example, in Fig. 2(a), the nesting vector of (0.3, 0.15) was identified using a (2×1) supercell. To alleviate the Fermi surface nesting, the new commensurate cell will have the periodicity of $[(2/0.3) \times (1/0.15)] \sim (6 \times 6)$. This will result in a long-range adsorption pattern and the (6×6) commensurate cell spanned 17.7×25.0 Å^2 on the surface. Electron-scattering surface state perturbation in this range remains detectable because the interaction on two-dimensional systems is more long-ranged than in the bulk. Predicted by Lau and Kohn, the interaction falls off as $1/R^3$ for the bulk cases and as $1/R^2$ for the 2D cases [18], whereby screening for the latter was insignificant [18]. The long-range interaction can be evidenced in the study of Cu/Cu(111) where the oscillatory behavior of Cu-Cu interaction extended beyond 60 Å [16]. Therefore, it is not unreasonable that we observe an energy lowering in the commensurate (6×6) cell.

In addition, the Fermi surface nesting can be removed by CO tilting along either the $\langle 1\bar{1}0 \rangle$ or $\langle 001 \rangle$ directions, respectively [along the sum or the difference of the Fermi nesting vectors found in Figs. 2(a), 2(c), and 2(d)]. Indeed, the Fermi surface nesting was slightly alleviated as shown in Fig. 2(b). Because of the geometrical constraint, the CO molecule is more likely to tilt along the $\langle 001 \rangle$ direction and the periodicity of the tilting motion along $\langle 1\bar{1}0 \rangle$ was determined by *ab initio* phonon calculations. The (2×1) cell with CO at $\Theta = 0.5$ was considered and the phonon dispersion could be obtained by including two additional cell images [(6×1) supercell].

For the short-range (4×1) adsorption pattern, Fig. 3(a) shows the phonon dispersion relation of the (2×1)-CO pattern at $\Theta = 0.5$ ML, and the phonon soft mode was located at the Brillouin zone edge [21] (see the

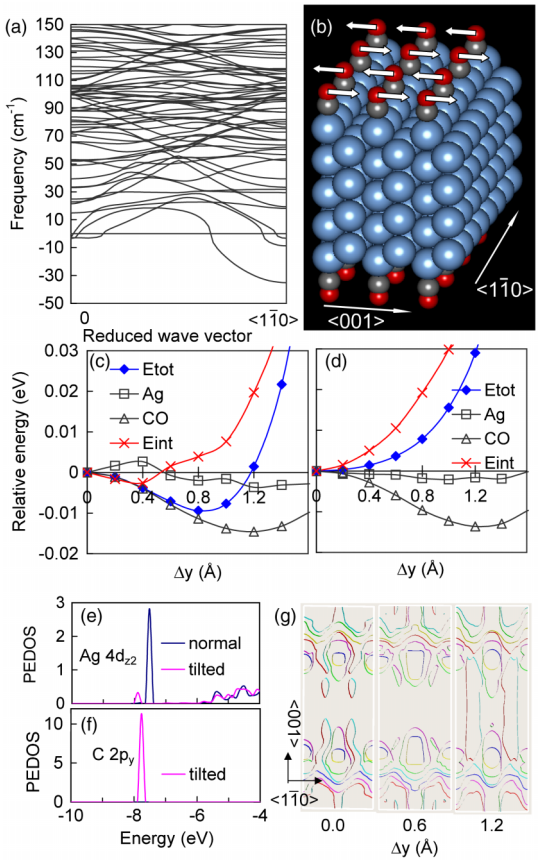

FIG. 3 (color online). (a) Phonon dispersion relation of (2×1) CO/Ag(110) at $\Theta = 0.5$ ML along $\langle 1\bar{1}0 \rangle$ direction. (b) Phonon soft mode at the Brillouin zone edge as found in (a). (c), (d) Energy decomposition analysis of CO on (2×1) Ag(110) at $\Theta = 0.5$ ML coverage and (4×1) Ag(110) at $\Theta = 0.25$ ML, respectively. (e), (f) Projected density of states of Ag and C atoms of the Ag-C bond at CO/(4×1) Ag(110) of $\Theta = 0.5$ ML, respectively, with CO normal (tilted) relative to the Ag(110) surfaces in blue (red) lines. (g) Evolution of two-dimensional Fermi surface of commensurate (4×1) cell at $\Theta = 0.5$ ML as a function of Δy.

Supplemental Material [13]). This implies a commensurate (4×1) ground state structure with adjacent CO molecules along the $\langle 1\bar{1}0 \rangle$ Ag row pointing alternatively to $\pm\langle 001 \rangle$ directions [Fig. 3(b)], in agreement with previous experimental findings [9]. Potential energy profiles of the CO bending mode along the $\langle 001 \rangle$ direction of a nine layer Ag(110) slab were examined [Figs. 3(c) and 3(d)]. The tendency of CO tilting depends on the CO line density along the $\langle 1\bar{1}0 \rangle$ direction. For CO adsorbed on the (2×1) Ag(110) surface, the CO orientation perpendicular to the surface is unstable and subject to deformation [Fig. 3(c)]. In contrast, a CO line density of 0.25 ML reveals a local minimum for the perpendicular CO orientation [Fig. 3(d)].

An energy decomposition analysis was performed which quantified the individual contributions by molecular or lattice distortions of pure CO or Ag(110) slabs, respectively. The individual energy terms [22] are depicted in Figs. 3(c) and 3(d) for CO/(2×1) Ag(110) and CO/(4×1) Ag(110), respectively. The CO tilting reduces quadrupole-quadrupole repulsive interactions between adjacent CO molecules and always with energy lowering on both the (2×1) and (4×1) Ag(110) surfaces. Therefore, the prior rationale was partially correct to assume that CO molecules would be tilted due to CO-CO quadrupolar repulsion. However, (i) the enhancement of the interaction energy between CO and the (2×1) Ag(110) substrate and (ii) interactions between CO molecules significantly influence the CO tilting orientation [Fig. 3(c)]. The former was corroborated by the Fermi level (i.e., electronic band energy) changes. In contrast, CO has not induced an electronic instability on the (4×1) pattern at $\Theta = 0.25$ ML and, therefore, the perpendicular CO orientation represents a local minimum [Fig. 3(d)]. A full geometry optimization was carried out for 0.5 ML CO on the 9 layer Ag(110) slab. The CO molecular axis is tilted along $\langle 001 \rangle$ by 27.6°, which is in excellent agreement with the previous ESDIAD results at 26° [9].

The alleviation of Fermi surface nesting is incorporated by the rehybridization of chemical bonds in deeper valence levels. Figures 3(e) and 3(f) illustrate the change of the density of states with respect to CO tilting orientation. The energy of the Ag-d_{z2} orbital is lowered by about 0.4 eV (from −7.52 to −7.92 eV), and a new C-p_y state is formed at the carbon atom [Fig. 3(f)]. The orbital rehybridization at the C atom results in a deviation of the Ag-C-O angle from its ideal angle of 180° corresponding to an s-p hybridization. Near the Fermi level, the intensity of projected density of states of Ag-d_{z2} has been reduced, causing a lowering of the Fermi level and the total energy. Figure 3(g) shows the change of the Fermi surface with respect to the CO tilting parameter Δy. The flat and parallel planes would be removed by CO tilting at $\Delta y = 0.6$ Å.

For the long-range adsorption pattern, the Fermi surface nesting can be removed by forming a commensurate (6×6) superstructure. We considered two (6×6) commensurate structures without further optimization for the (2×1) [Fig. 1(a)] and (2×2) [Fig. 1(b)] cells, denoted by (6×6)-a [Fig. 4(a)] and (6×6)-b [Fig. 4(b)], respectively. The formation of the commensurate phase resulted in an energy lowering [23]. The energy lowering was 1.9 and 4.8 meV/CO for (6×6)-a and (6×6)-b, respectively. When compared with the energy lowering of the (4×1) structure of about 7.5 meV/CO, the tilted CO geometry is more favorable at low temperature.

Despite the small magnitude in energy lowering in commensurate (6×6) structures, the change of chemical bonding is substantial. A comparison of the normalized electronic density of states of (6×6)-a and (2×1) cells is shown in Fig. 4(c). New peaks formed by the s-p_y hybridization and a C-p_x state appear, which correspond

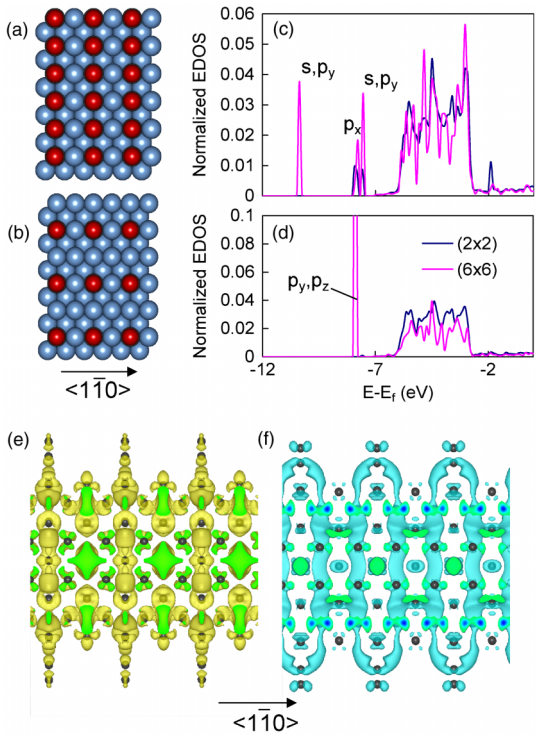

FIG. 4 (color online). (a), (b) Structures of (6×6)-a and (6×6)-b. (c) Electronic density of states (EDOS) of (2×1) CO/Ag(110) at $\Theta = 0.5$ ML (blue) and that of (6×6)-a CO/Ag(110) at $\Theta = 0.5$ ML (red). (d) Electronic density of states of (2×2) CO/Ag(110) at $\Theta = 0.25$ ML (blue) and that of (6×6)-b CO/Ag(110) at $\Theta = 0.25$ ML (red). (e), (f) Electron accumulation or depletion of (6×6)-b CO/Ag(110) at $\Theta = 0.25$ ML, respectively. In (e) and (f), the isosurface of the electron density is 4×10^{-6} a.u.

to a localization of electrons at the CO molecule. Similarly, Fig. 4(d) shows the rehybridization of the (6×6)-b structure of CO/Ag(110) by forming molecular orbitals of C-O at deeper levels via Cp_y-Op_y and Cp_z-Op_z interactions, respectively. Overall, the shift of the electron density of states toward the deeper valence level accounts for the lowering of the total energy. To illustrate electronic density changes due to the formation of the commensurate phase, the electron density of the commensurate (6×6)-b structure was subtracted from the electron density of the repeated images of the (2×2) cell, which shows electron accumulation at the C and O atoms [Fig. 4(e)]. This results in Ag-C bond weakening, which is also revealed by detection of electron depletion for the metal-$d \rightarrow$ CO-$2\pi^*$ donation [Fig. 4(f)]. Thus, the alleviation of the Fermi surface nesting can also be achieved by the formation of the (6×6) commensurate structure.

In general, the substrate mediated interaction is on the order of 0.005–0.1 eV while the chemisorption strength falls within the range 0.5–10 eV [15]. The adsorption geometry of CO and/or other diatomic polar molecules on metal surfaces would be governed by a delicate balance of these different types of interaction. CO is weakly adsorbed on precious metals and therefore its adsorption geometry would be influenced by substrate mediated interaction on Ag(110), Pt(110), and probably on Au(110). Fermi surface nesting should also be expected in other bigger and more complex molecules on metal surfaces like Cu-PBP on Ag(111) [15].

In summary, we have identified two competing substrate relaxation mechanisms of the CO/Ag(110) system. Energetically, the short-range (4×1) pattern with tilted CO is preferred. The short-range relaxation leads to CO tilting and the alleviation of Fermi surface nesting. The long-range relaxation leads to the commensurate (6×6) structure in which CO has a weaker covalent interaction with the Ag(110) substrate while the electrons are localized at the C-p and O-p orbitals. Our findings suggest that the adsorption pattern and the adsorbate dynamics can be traced back to the interactions of heavy electrons by Fermi surface nesting. This approach should also be applicable to explain the interfacial dynamics of complex adsorbate on metal surface systems such as sulphur on Au(111), 1-adamantaneselenolate self-assembled monolayers on Au(111), and Cu-PBP on Ag(111) [11,15,24].

We acknowledge Neil Drummond, Rolf Heid, and Steve C. F. Au-Yeung for useful discussions. W.-L. Y. acknowledges the IHPC Independent Investigatorship and A*STAR Computational Resource Centre (A*CRC) for computing facilities.

*Corresponding author.
yimwl@ihpc.a-star.edu.sg

[1] F. Schreiber, Prog. Surf. Sci. **65**, 151 (2000); G. E. Poirier, Langmuir **15**, 1167 (1999); N. Camillone, T. Y. B. Leung, P. Schwartz, P. Eisenberger, and G. Scoles, Langmuir **12**, 2737 (1996).
[2] P. Maksymovych, D. C. Sorescu, K. D. Jordan, and J. T. Yates, Science **322**, 1664 (2008); M. Feng, P. Cabrera-Sanfelix, C. W. Lin, A. Arnau, D. Sánchez-Portal, J. Zhao, P. M. Echenique, and H. Petek, ACS Nano **5**, 8877 (2011).
[3] G. Pirug and H. P. Bonzel, Surf. Sci. **405**, 87 (1998); S. L. Horswell, A. L. N. Pinheiro, E. R. Savinova, B. Pettinger, M.-S. Zei, and G. Ertl, J. Phys. Chem. B **108**, 18640 (2004).
[4] J. W. He, W. K. Kuhn, and D. W. Goodman, Chem. Phys. Lett. **177**, 109 (1991).
[5] S. R. Bare, P. Hofmann, and D. A. King, Vacuum **31**, 463 (1981); P. Hofmann, S. R. Bare, N. V. Richardson, and D. A. King, Solid State Commun. **42**, 645 (1982).
[6] C. W. Bauschlicher, Chem. Phys. Lett. **115**, 535 (1985).
[7] D. A. Wesner, F. P. Coenen, and H. P. Bonzel, Phys. Rev. Lett. **60**, 1045 (1988); Phys. Rev. B **39**, 10770 (1989).
[8] H. Kato, H. Okuyama, S. Ichihara, M. Kawai, and J. Yoshinobu, J. Chem. Phys. **112**, 1925 (2000).
[9] J. G. Lee, S.-H. Hong, J. Ahner, X. Zhao, L. Chen, J. K. Johnson, and J. T. Yates, Chem. Phys. Lett. **418**, 90 (2006).

[10] E. C. H. Sykes, B. A. Mantooth, P. Han, Z. J. Donhauser, and P. S. Weiss, J. Am. Chem. Soc. **127**, 7255 (2005).

[11] J. N. Hohman, M. Kim, B. Schüpbach, M. Kind, J. C. Thomas, A. Terfort, and P. S. Weiss, J. Am. Chem. Soc. **133**, 19422 (2011).

[12] We used the VASP code to perform calculations within density functional theory; see G. Kresse and J. Furthmüller, Comput. Mater. Sci. **6**, 15 (1996); Phys. Rev. B **54**, 11169 (1996). The structural stability or instability was tested by AIMD using the primitive unit cell. The AIMD was performed by a canonical ensemble at 25 K for 10 ps which was controlled by a Nosé-Hoover thermostat; see S. Nosé, J. Chem. Phys. **81**, 511 (1984).

[13] See Supplemental Material at http://link.aps.org/supplemental/10.1103/PhysRevLett.110.196101 for computational parameters.

[14] W. L. Yim and T. Klüner, Phys. Rev. B **85**, 035435 (2012).

[15] P. Han and P. S. Weiss, Surf. Sci. Rep. **67**, 19 (2012).

[16] J. Repp, F. Moresco, G. Meyer, K. H. Rieder, P. Hyldgaard, and M. Persson, Phys. Rev. Lett. **85**, 2981 (2000).

[17] P. T. Sprunger, L. Petersen, E. W. Plummer, E. Laegsgaard, and F. Besenbacher, Science **275**, 1764 (1997); M. Kralj, M. Milun, and P. Pervan, Surf. Sci. **557**, 208 (2004).

[18] K. H. Lau and W. Kohn, Surf. Sci. **75**, 69 (1978).

[19] Ultrasoft pseudopotentials were adopted by using the QUANTUM ESPRESSO software package; see S. Baroni, A. D. Corso, S. d. Gironcoli, and P. Giannozzi, http://www.pwscf.org.

[20] J. Schafer, D. Schrupp, E. Rotenberg, S. D. Kevan, and R. Claessen, Appl. Phys. A **80**, 965 (2005).

[21] *Ab initio* phonon calculations were carried out by using the direct force constant approach; see W. L. Yim and T. Klüner, J. Phys. Chem. C **115**, 3286 (2011); K. Parlinski, Z. Q. Li, and Y. Kawazoe, Phys. Rev. Lett. **78**, 4063 (1997); a supercell containing three primitive unit cells along the $\langle 1\bar{1}0\rangle$ direction of the Ag(110) slab was used.

[22] The energy is represented as $E_{\mathrm{tot}}(\Delta y) = E_{\mathrm{pure\,CO}}(\Delta y) + E_{\mathrm{pure\,Ag\,slab}}(\Delta y) + E_{\mathrm{int}}(\Delta y)$. Δy is the displacement of oxygen relative to the substrate Ag atom along the $\langle 001\rangle$ direction. $E_{\mathrm{tot}}(\Delta y)$ is the energy of the optimized CO/Ag(110) structure, whereas $E_{\mathrm{pure\,CO}}(\Delta y)$ and $E_{\mathrm{pure\,Ag\,slab}}(\Delta y)$ are the energies of the CO and Ag(110) fragments which are taken from CO/Ag(110) without further optimization. Finally, $E_{\mathrm{int}}(\Delta y)$ is the interaction energy of the fragments.

[23] $E_{\mathrm{lowering}} = E_{(6\times6)\text{-}a} - 18E_{(2\times1)}$ when referenced to the (2×1) cell, and $E_{\mathrm{lowering}} = E_{(6\times6)\text{-}b} - 9E_{(2\times2)}$ when referenced to the (2×2) cell.

[24] M. Yu, H. Ascolani, G. Zampieri, D. P. Woodruff, C. J. Satterley, R. G. Jones, and V. R. Dhanak, J. Phys. Chem. C **111**, 10904 (2007).